

Influence of differential stress on the galvanic interaction of pyrite–chalcopyrite

Qingyou Liu · Yanqing Zhang · Heping Li

Received: 15 February 2012 / Revised: 22 March 2012 / Accepted: 25 March 2012 / Published online: 13 April 2012
© Springer-Verlag 2012

Abstract The effect of stress action on pyrite–chalcopyrite galvanic corrosion was investigated using polarization curves and electrochemical impedance spectroscopy (EIS) measurements. When stress increased from 0 to 4×10^5 Pa, the corrosion current density of pyrite–chalcopyrite increased from 5.678 to 6.719 $\mu\text{A cm}^{-2}$, and the corrosion potential decreased from 281.634 to 270.187 mV, accompanied by a decrease in polarization resistance from 25.09 to 23.79 $\Omega\text{-cm}^2$. EIS results show there have three time constants in the Nyquist diagrams, which indicated the presence of different steps during the corrosion process. Stress dramatically enhanced pyrite–chalcopyrite galvanic corrosion by affecting the $\text{Cu}_{1-x}\text{Fe}_{1-y}\text{S}_2$ film and the double layer, whereas had little impact on the adsorption species. When the stress changed from 0 to 4×10^5 Pa, the pore resistance and capacitance of the $\text{Cu}_{1-x}\text{Fe}_{1-y}\text{S}_2$ film, R_p and Q_p , changed by 25.72 and 72.28 %, respectively. The adsorption species resistance, R_{sl} , and capacitance, Q_{sl} , only changed by 9.77 and 2.31 %, respectively.

Keywords Pyrite · Chalcopyrite · Galvanic corrosion · Polarization curves · EIS · Differential stress

Introduction

As the most common and exploitable sulfide minerals, pyrite and chalcopyrite are often in contact with each other and

coexist together. When an electrolyte is present, galvanic interactions occur, and these interactions play an important role in the material characteristics. It has been widely accepted that galvanic effects may be one of the most important electrochemical factors that govern the dissolution rate of sulfide minerals [1]. There are a large number of reports in the literature that explain the galvanic corrosion of pyrite–chalcopyrite using potentiodynamic polarization measurements [2], cyclic voltammetry [3], microelectrophoresis [4], and Galvanox™ [5, 6]. Various surface techniques have also been used, such as scanning electron microscopy [7], energy dispersive X-ray analysis [2], X-ray photoelectron spectroscopy [8–10], and X-ray diffraction [11].

To our knowledge, no quantitative data have been reported on galvanic interactions between pyrite and chalcopyrite under stress. Stress on these sulfide minerals is caused by both human exploitation and natural geochemical processes. As a result of stress, strain energy changes into electrochemical energy and significantly influences the electrochemical behavior of these sulfide minerals. In the mine environmental field, Sprocati et al. [12] found that tectonic stress increased galvanic interactions and induced metal pollution and acidic mine drainage in an abandoned mine. In the hydrometallurgy and mineral processing field, the use of high-energy mills created a dramatic change in the structure and surface properties of the solids [13, 14]. Stress relaxation caused changes in the reactivity of the solid substances, which is known as mechanical activation [15]. The mechanical energy was partially transferred to the particles, and its effects included a multitude of elementary physicochemical micro- and macroprocesses. Furthermore, it is well-known that much of the Earth's crust is under stress. Khilyuk et al. [16] noted that excessive accumulation of stress is the primary cause of all seismic events. Ubiquitous in the Earth's crust, FeCl_3 is not only a common electrolyte but also deeply affects the electrochemical behavior of metal sulfides. It is the most used media to leach sulfide [17], the most abundant component of

Q. Liu · Y. Zhang · H. Li (✉)
Laboratory for High Temperature & High Pressure
Study of the Earth's Interior, Institute of Geochemistry,
Chinese Academy of Sciences,
Guiyang 550002, China
e-mail: liheping123@yahoo.com

Y. Zhang
Graduate University of Chinese Academy of Sciences,
Beijing 100039, China

the Earth's crust [18], and the most common component of mine water [19, 20]. Therefore, the aim of this work is to study the electrochemical response of a massive pyrite–chalcopyrite couple in an FeCl_3 solution under differential stress conditions to obtain quantitative electrochemical parameters. These observations will provide the experimental basis from which to derive a better understanding of the behavior of pyrite–chalcopyrite couples in pressure solutions, under mechanical activation and under geological stresses.

Experimental

Samples, reagents, and instrumentation

Two dense, compact masses of natural pyrite (origin: Yunfu mine, China) and chalcopyrite (origin: Daye mine, China) were used as experimental samples. The samples were cut and shaped into $10 \times 10 \times 40$ -mm blocks. Reflected light microscopy and X-ray diffraction analysis indicated that the samples existed in a pure, homogeneous phase. Electron microprobe analysis confirmed that the pyrite's Fe and S (in weight percent) content were 46.89 and 52.96 %, respectively, whereas chalcopyrite's Fe, Cu, and S content (in weight percent) were 30.70, 34.04 and 34.67 %, respectively. Before the experiments, fresh electrode surfaces were prepared using metallographic abrasive papers, and the surfaces were cleaned with filter paper and rinsed with acetone until clean. After each experiment, the used electrodes were repolished and reused.

The electrolyte was prepared from analytical grade chemicals and doubly distilled water. During all experiments, the electrochemical cell (made of rigid polytetrafluoroethylene with a capacity of 60 mL) was filled with FeCl_3 solution without purging the dissolved oxygen.

All mineral stress experiments were performed on an electronic universal testing machine controlled by computer. Two resistance strain gauges were installed on the chalcopyrite sample's axial and lateral surfaces. Depending on the dynamic and static strain testing system, data for axial stress, axial strain, and lateral strain were collected. To compare rapid and continuously varying axial stresses (0, 2.0×10^5 , and 4.0×10^5 Pa), polarization curves and electrical impedance spectroscopy data were collected. The experiments were conducted using a stationary electrode in an air-conditioned room at 25 ± 1 °C.

Polarization curves and EIS measurements

The polarization curves were measured with a Parstat-2263 equipped with a PowerSuite system. The working and counter electrodes that were used to study pyrite and chalcopyrite had

exposed areas of 4 cm^2 . The reference electrode was a saturated calomel electrode (SCE). The potentials are quoted with respect to the SCE. The polarization scan was from -250 mV relative to the open circuit potential (E_{OC}) to $+250 \text{ mV}$ relative to the E_{OC} at a rate of 1 mV/s . The data were recorded after 1 h of immersion in the working solution. The experimental control and the data analysis were performed using the PowerCorr software created by Parstat Princeton Applied Research.

Electrochemical impedance spectroscopy (EIS) experiments were performed at an open circuit potential in the 2×10^5 - to 0.01 -Hz frequency range. The amplitude of the sinusoidal voltage was 5 mV-rms . The equivalent circuit model for fitting the AC impedance was evaluated by employing the ZSimpWin (Version 3.10) software from PAR.

Results and discussion

Linear polarization measurements

Linear polarization measurements were used to study the corrosion behavior of the pyrite–chalcopyrite galvanic system in contact with a naturally aerated 0.0010-mol L^{-1} FeCl_3 solution under different elastic axial stresses (0, 2×10^5 , 4×10^5 Pa). Specifically, the target stress (2×10^5 , 4×10^5 Pa) will be quickly reached via an elastic strain process and kept at that stress until the experiment is finished. The data were recorded when the chalcopyrite electrode reached a steady state. Their Tafel plots are presented in Fig. 1. A close look at Fig. 1 reveals some details about the chalcopyrite anodic behavior. With increasing stress, the anode curve became steeper, and the entire curve exhibited an obvious shift in the negative direction along the vertical axis. According to the linear polarization Eqs. (1), (2), and

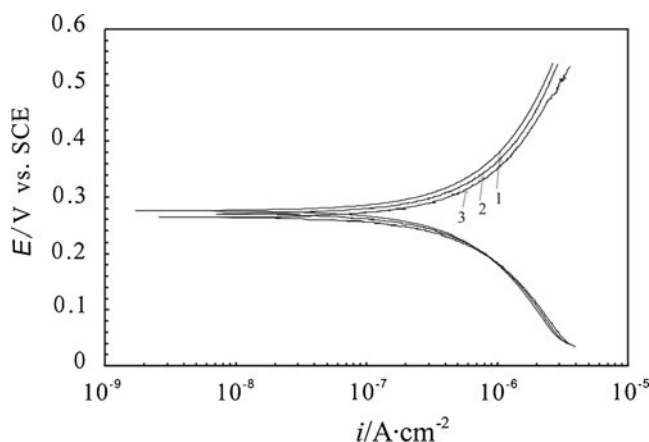


Fig. 1 Tafel plots for FeS_2 – CuFeS_2 galvanic corrosion under differential stresses in $0.0010 \text{ mol L}^{-1}$ FeCl_3 solutions. 1 0 Pa, 2 2.0×10^5 Pa, and 3 4.0×10^5 Pa

Table 1 Electrochemical parameters of FeS₂–CuFeS₂ galvanic corrosion in 0.0010 M FeCl₃ solutions under differential stresses

Chalcopyrite stress (10 ⁵ Pa)	<i>E</i> _{corr} (mV)	<i>i</i> _{corr} (μA·cm ⁻²)	<i>b</i> _a (mV)	<i>b</i> _c (mV)	Transfer coefficient		Number of electron transfer (<i>n</i>)	<i>R</i> _p (Ω·cm ²)
					α	β		
0	281.634	5.678	568.731	773.157	0.424	0.576	0.482	25.09
2	275.749	5.966	601.245	778.245	0.436	0.564	0.466	24.72
4	270.187	6.719	666.883	819.607	0.449	0.551	0.430	23.79

*E*_{corr} corrosion potential, *i*_{corr} corrosion current density, *b*_a anode Tafel slope, *b*_c cathode Tafel slope

(3), several kinetic parameters, such as the corrosion current density, Tafel slope, transfer coefficient, and number of electrons transferred, were calculated using the PAR software.

$$I = i_{\text{corr}} \left[\exp \frac{2.303(E - E_{\text{corr}})}{b_a} - \exp \frac{-2.303(E - E_{\text{corr}})}{b_c} \right] \tag{1}$$

$$b_a = \frac{2.303RT}{\beta nF}, b_c = \frac{2.303RT}{\alpha nF} \tag{2}$$

$$\alpha = 1 - \beta \tag{3}$$

Furthermore, the polarization resistance values, *R*_p, were calculated from the Stern–Geary equation [21]:

$$I_{\text{corr}} = \frac{b_a b_c}{2.3(b_a + b_c)} \cdot \frac{1}{R_p} \tag{4}$$

The linear polarization experimental results are listed in Table 1. It can be observed that, with increasing stress from 0 to 4 × 10⁵ Pa, the pyrite–chalcopyrite galvanic interaction corrosion current density increased from 5.678 to 6.719 μA cm⁻². However, the corrosion potential became more negative and decreased from 281.634 to 270.187 mV. Additionally, the polarization resistance values, *R*_p, decreased from 25.09 to 23.79 Ω·cm². These results showed that increased stress benefited the pyrite–chalcopyrite electrochemical interaction and induced more galvanic corrosion.

These phenomena provided strong evidence for the enhancement of pyrite–chalcopyrite galvanic corrosion in the presence of a differential stress. Further, it should be noted that the transfer coefficient and the number of electron transferred, which are indicative of the electrode reaction mechanism [22], did not significantly change under differential stresses. These results suggested that the addition of differential stresses simply facilitated electron transfer but did not change the pyrite–chalcopyrite corrosion mechanism. From the stress–electrode potential discussion, one can easily understand that stress causes a conversion of the strain energy into electrochemical energy, which decreases the chalcopyrite electrode potential and results in an increase in galvanic corrosion. Our results clearly showed how differential stress affected the pyrite–chalcopyrite anode electrochemical interaction from a macroscopic perspective. To better understand how and to what extent differential stress affected the pyrite–chalcopyrite anodic electrochemical interaction from a microscopic perspective, impedance studies were performed.

EIS measurements

EIS measurements are often used to obtain information about the properties of a system, such as the presence of defects, reactivity of an interface, adhesion properties, and barrier properties. Knowledge of these parameters is important when predicting corrosion behavior [23]. In this work, EIS was used to study the microkinetics properties of the

Fig. 2 Bode plots and phase angles (a), Nyquist impedance spectra (b), and equivalent circuit (c) for FeS₂–CuFeS₂ galvanic corrosion under differential stresses in 0.0010 mol L⁻¹ FeCl₃ solutions. Where 0 Pa (filled diamonds), 2.0 × 10⁵ Pa (filled triangles), and 4.0 × 10⁵ Pa (filled circles) experimental and simulated (solid lines)

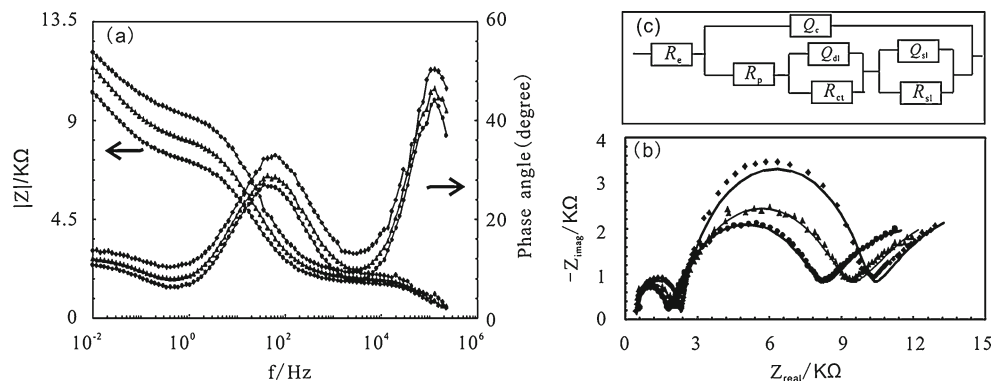


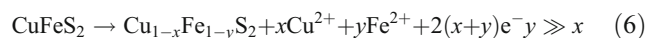
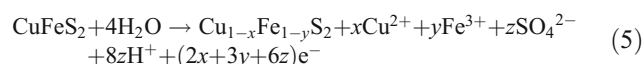
Table 2 Impedance parameters of FeS₂–CuFeS₂ galvanic corrosion in 0.0010 M FeCl₃ solutions under differential stresses

Chalcopyrite stress (10 ⁵ Pa)	R_p (Ω·cm ²)	R_{ct} (Ω·cm ²)	R_{dl} (Ω·cm ²)	Q_p		Q_{dl}		Q_{sl}	
				$Y_{0,1}$ (S·cm ⁻² ·s ⁻ⁿ)	n_1	$Y_{0,2}$ (S·cm ⁻² ·s ⁻ⁿ)	n_2	$Y_{0,3}$ (S·cm ⁻² ·s ⁻ⁿ)	n_3
0	1,730	7,291	8,221	2.843E-9	0.9603	3.68E-6	0.7376	9.014E-4	0.6355
2	1,513	6,463	7,801	3.325E-9	0.9585	4.912E-6	0.7244	9.101E-4	0.6068
4	1,285	5,656	7,418	4.898E-9	0.9331	5.527E-6	0.7154	9.222E-4	0.6044

covering layer and the double layer of a pyrite–chalcopyrite galvanic electrode in contact with a naturally aerated 0.0010-mol L⁻¹ FeCl₃ solution under different elastic axial stresses (0, 2.0×10⁵, 4.0×10⁵ Pa). Specifically, the target stress (2×10⁵, 4×10⁵ Pa) will be quickly reached via an elastic strain process and kept at that stress until the experiment is finished. The data collection was performed after 1 h of stabilization.

Figure 2 shows the Bode plot diagram and a typical Nyquist diagram for pyrite–chalcopyrite obtained in a 0.0010-mol L⁻¹ FeCl₃ solution under different elastic axial stresses. Three time constants were clearly observed from the three distorted capacitive loops. The complexity of the Nyquist diagrams indicated the presence of different steps during the corrosion process. Considering that there are three time constants, the analysis of the impedance diagram is presented in Fig. 2c. R_c is the combined resistance of the electrolyte and other ohmic resistances, R_{ct} is the charge transfer resistance, and Q_p corresponds to the capacitance of the coating layer. Previous studies [24, 25] show that electrochemical reactions on the surface of chalcopyrite electrodes in different potential intervals had different passive layer. From OCP to ~0.5 V (vs. SCE), the coating layer is Cu_{1-x}Fe_{1-y}S₂. Based on the above studies, and considering the potential in our EIS experiments that was addressed in this potential region, we conclude that the coating layer in this work is Cu_{1-x}Fe_{1-y}S₂, which created via the reactions shown in interaction (5) or (6) [24, 26]. R_p is the pore resistance of this film. Q_{dl} is the double layer capacitance. R_{sl} and Q_{sl} refer to the adsorption species, such as iron-containing compounds. Such a model has previously been used by Velásquez et al. [27] to model the interfacial behavior of chalcopyrite in alkaline solutions. Furthermore, Q_c , Q_{sl} , and Q_{dl} were modeled by a constant phase element (CPE) [28]. The CPE is a distributed element defined as $Q=1/Kp^n$, $0 \leq n \leq 1$. In this expression, n is a dimensionless number and defines how different the interface is from an

ideal capacitor; when $n=1$, the capacitance is considered ideal. K is a constant whose units are in farads second ^{$n-1$} per square centimeter, and $p=j\omega$ with $\omega=2\pi f$. Q is equivalent to the impedance when the capacitance is $C=K(2pf)^{n-1}$. Therefore, the CPE behaves as a capacitance that varies with the frequency. This modification to the ideal capacitance has already been explained by distribution effects [29], porosity [30], and the distribution of interfacial capacitances [31].



The EIS experimental results are shown in Table 2. On the whole, the increase in stress was accompanied by a decrease in the resistance parameter (R_p , R_{ct} , and R_{sl}) and exponent (n_1 , n_2 , n_3) values and an increase in the capacitance parameter ($Y_{0,1}$, $Y_{0,2}$, $Y_{0,3}$) values. Generally, the resistance parameter values, R , represents to what extent charge can transfer to a corresponding interface. The capacitance parameter, Y_0 , characterizes the ions and to what extent they can diffuse through and accumulate on a corresponding layer. The exponent n represents the roughness of the surface. Larger resistance and capacitance parameter values and a smaller exponent n value indicate that the kinetics of the electrochemical process and the porosity of the film on the electrode surface increase with increasing stress. According to the above stress–electrode potential discussion, when stress increases, the chalcopyrite electrode potential decreases.

To more thoroughly understand how stress affects the pyrite–chalcopyrite electrochemical interaction, we defined a variation of the resistance or capacitance parameter value, Δx .

$$\Delta x = \frac{x_1 - x_0}{x_0} \cdot 100 \% \quad (7)$$

Table 3 Variation of the resistance parameter and capacitance parameter value

Chalcopyrite stress (10 ⁵ Pa)	ΔR_p (%)	ΔR_{ct} (%)	ΔR_{dl} (%)	$\Delta Y_{0,1}$ (%)	$\Delta Y_{0,2}$ (%)	$\Delta Y_{0,3}$ (%)
2	12.54	11.36	5.11	16.95	33.48	0.97
4	25.72	22.42	9.77	72.28	50.19	2.31

where x_0 is the resistance or capacitance parameter value without stress and x_1 is the resistance or capacitance parameter value with 2×10^5 or 4×10^5 Pa of stress. Based on Eq. (7), we derived the variation of resistance and capacitance parameter values and provided them in Table 3. From the data in Table 3, when stress increased from 0 to 4×10^5 Pa, it is clear that: (1) the pore resistance of $\text{Cu}_{1-x}\text{Fe}_{1-y}\text{S}_2$ film, R_p , decreased by 25.72 % and coating film capacitance, Q_c , increased by 72.28 %, respectively; (2) the charge transfer resistance, R_{ct} , decreased by 22.42 % and double layer capacitance, Q_{dl} , increased by 50.19 %, respectively; and (3) the adsorption species resistance, R_{sl} , decreased by 9.77 % and the adsorption species capacitance, Q_{sl} , increased by 2.31 %, respectively.

As already mentioned above, the Q_{dl}/R_{ct} pair represents the charge transform capacitive and resistance behavior in the double layer region. In this work, increased stress resulted in higher capacitance and lower resistance of the double layer, indicating the charges are more easily diffused through the electric double layers, that is the chalcopyrite electrode electrochemical dissolution changes easier. In addition, the Q_c/R_p pair represents the capacitive and resistive behavior of the coating layer, and their values reveal to what extent they can inhibit mineral dissolution. Similarly, higher capacitance and lower resistance of the film indicate the film had less capability to inhibit mineral dissolution. At last, the Q_{sl}/R_{sl} pair represents the capacitive and resistive behavior of the adsorption species, and their values reveal to what extent the species can adsorb on the mineral surface. The results reveal that higher stresses are a disadvantage to species adsorption.

Conclusions

The electrochemical behavior of the pyrite–chalcopyrite galvanic cell in an FeCl_3 solution under differential stress was studied using polarization curves and electrical impedance spectroscopy. Two conclusions can be drawn from this research:

1. Linear polarization results showed that stress can speed up the electrochemical pyrite–chalcopyrite galvanic corrosion. When stress increased from 0 to 4×10^5 Pa, the corrosion current density increased from 5.678 to $6.719 \mu\text{A cm}^{-2}$. The corrosion potential changed from 281.634 to 270.187 mV and was accompanied by a decrease in the polarization resistance value from 25.09 to $23.79 \Omega \cdot \text{cm}^2$.
2. EIS experimental results showed that stress enhanced pyrite–chalcopyrite galvanic corrosion mainly by affecting the properties of the $\text{Cu}_{1-x}\text{Fe}_{1-y}\text{S}_2$ film and the double layer; however, stress had little effect on the adsorption species. When stress changed from 0 to $4 \times$

10^5 Pa, the pore resistance, R_p , and capacitance, Q_p , of the $\text{Cu}_{1-x}\text{Fe}_{1-y}\text{S}_2$ film changed by 25.72 and 72.28 %, respectively. The adsorption species resistance, R_{sl} , and capacitance, Q_{sl} , only changed by 9.77 and 2.31 %, respectively.

Acknowledgments This work was financially supported by National Natural Science Foundation of China (40803017), Large-scale Scientific Apparatus Development Program of Chinese Academy of Sciences (YZ200720), and Municipal Science and Technology Foundation of Guizhou Province, China (No. 2008GZ02240), Key Technologies R & D Program of Guizhou Province, China (SY [2011] 3088), and West Light Foundation Doctor Cultivate Progress Foundation of the Chinese Academy of Sciences.

References

1. Majima H, Peter E (1968) Electrochemistry of sulphide dissolution in hydrometallurgical systems. The VIII International Mineral Processing Congress. Leningrad, pp 13
2. Metha AP, Murr LE (1983) Fundamental studies of the contribution of galvanic interaction to acid-bacterial leaching of mixed metal sulfides. *Hydrometallurgy* 9:235–256
3. Ekmekçi Z, Demirel H (1997) Effects of galvanic interaction on collectorless flotation behaviour of chalcopyrite and pyrite. *Int J Miner Process* 52:31–48
4. Chandraprabha MN, Natarajan KA, Somasundaran P (2005) Selective separation of pyrite from chalcopyrite and arsenopyrite by biomodulation using *Acidithiobacillus ferrooxidans*. *Int J Miner Process* 75:113–122
5. Nazari G, Dixon DG, Dreisinger DB (2011) Enhancing the kinetics of chalcopyrite leaching in the Galvanox™ process. *Hydrometallurgy* 105:251–258
6. Nazari G, Dixon DG, Dreisinger DB (2012) The role of galena associated with silver-enhanced pyrite in the kinetics of chalcopyrite leaching during the Galvanox™ process. *Hydrometallurgy* 111–112:35–45
7. Berry VK, Murr LE, Hiskey JB (1978) Galvanic interaction between chalcopyrite and pyrite during bacterial leaching of low-grade waste. *Hydrometallurgy* 3:309–326
8. He SH, Skinner W, Fornasiero D (1986) Effect of oxidation potential and zinc sulphate on the separation of chalcopyrite from pyrite. *Int J Miner Process* 80:169–176
9. McCarron JJ, Walker GW, Buckley AN (1990) An X-ray photoelectron spectroscopic investigation of chalcopyrite and pyrite surfaces after conditioning in sodium sulfide solutions. *Int J Miner Process* 30:1–16
10. Peng YJ, Grano S, Fornasiero D, Ralston J (2003) Control of grinding conditions in the flotation of chalcopyrite and its separation from pyrite. *Int J Miner Process* 69:87–100
11. Javad Koleini SM, Aghazadeh V, Sandström Å (2011) Acidic sulphate leaching of chalcopyrite concentrates in presence of pyrite. *Miner Eng* 24:381–386
12. Sprocati AR, Alisi C, Segre L, Tasso F, Galletti M, Cremisini C (2006) Investigating heavy metal resistance, bioaccumulation and metabolic profile of a metallophile microbial consortium native to an abandoned mine. *Sci Total Environ* 366:649–658
13. Baláz P (2000) Extractive metallurgy of activated minerals, 1st edn. Elsevier, Amsterdam, pp 35–77
14. Tkacova K (1989) Mechanical activation of minerals, 1st edn. Elsevier, Amsterdam, pp 26–38

15. Boldyrev VV, Tkacova K (2000) Mechanochemistry of solids: past, present, and prospects. *J Mater Synth Process* 8:121–132
16. Khilyuk LF, Chilingar GV, Robertson JO, Endres B (2000) Messages from the Earth's crust. In *Gas migration*. Elsevier, Amsterdam, pp 163–187
17. Dutrizac JE (1992) The leaching of sulphide minerals in chloride media. *Hydrometallurgy* 29:1–45
18. Bailey RA, Clark HM, Ferris JP, Krause S, Strong RL (2002) The earth's crust. In *Chemistry of the environment*, 2nd edn. Elsevier, Amsterdam, pp 443–482
19. Bowell RJ, Bruce I (1995) Geochemistry of iron ochres and mine waters from Levant Mine, Cornwall. *Appl Geochem* 10:237–250
20. Silva EFD, Bobos I, Matos JX, Patinha C, Reis AP, Fonseca EC (2009) Mineralogy and geochemistry of trace metals and REE in volcanic massive sulfide host rocks, stream sediments, stream waters and acid mine drainage from the Lousal mine area (Iberian Pyrite Belt, Portugal). *Appl Geochem* 24:383–401
21. Gonzalez-Rodriguez JG, Mejia E, Lucio-Garcia MA, Salinas-Bravo VM, Porcayo-Calderon J, Martinez-Villaf A (2009) An electrochemical study of the effect of Li on the corrosion behavior of Ni₃Al intermetallic alloy in molten (Li+K) carbonate. *Corros Sci* 51:1619–1627
22. Liu JS (2002) Bioextraction and corrosion electrochemistry of sulfide minerals. Ph.D. thesis, Central South University pp. 34–38
23. Bonora PL, Deflorian F, Fedrizzi L (1996) Electrochemical impedance spectroscopy as a tool for investigating underpaint corrosion. *Electrochim Acta* 41:1073–1082
24. Nava D, Gonzalez I (2006) Electrochemical characterization of chemical species formed during the electrochemical treatment of chalcopyrite in sulfuric acid. *Electrochim Acta* 51:5295–5442
25. Ghahremaninezhad A, Asselin E, Dixon DG (2010) Electrochemical evaluation of the surface of chalcopyrite during dissolution in sulfuric acid solution. *Electrochim Acta* 55:5041–5056
26. Hackl RP, Dreisinger DB, Peters E, King JA (1995) Passivation of chalcopyrite during oxidative leaching in sulfate media. *Hydrometallurgy* 39:25–48
27. Velásquez P, Leinen D, Pascual J, Ramos-Barrado JR, Grez P, Gómez H, Schrebler R, RÍo RD, Córdova R (2005) A chemical, morphological, and electrochemical (XPS, SEM/EDX, CV, and EIS) analysis of electrochemically modified electrode surfaces of natural chalcopyrite (CuFeS₂) and pyrite (FeS₂) in alkaline solutions. *J Phys Chem B* 109:4977–4988
28. Macdonald JR (1985) Generalizations of “universal dielectric response” and a general distribution-of-activation-energies model for dielectric and conducting systems. *J Appl Phys* 58:1971–1978
29. Brug GJ, Van-den-Eden ALG, Sluyters-Rehbach M, Sluyters HJ (1984) The analysis of electrode impedances complicated by the presence of a constant phase element. *J Electroanal Chem* 176:275–295
30. Gassa LM, Vilche JR, Ebert M, Juttner K, Lorenz WJ (1990) Electrochemical impedance spectroscopy on porous electrodes. *J Appl Electrochem* 20:677–685
31. Pajkossy T (1997) Capacitance dispersion on solid electrodes: anion adsorption studies on gold single crystal electrodes. *Solid State Ionics* 94:123–129